THESIS FOR THE DEGREE OF LICENTIATE OF ENGINEERING

The impact of loading-induced stress variation on the seismicity of active faults

YITING CAI

Department of Space, Earth and Environment
Onsala Space Observatory
CHALMERS UNIVERSITY OF TECHNOLOGY
Gothenburg, Sweden 2023

The impact of loading-induced stress variation on the seismicity of active faults
YITING CAI

Department of Space, Earth and Environment
Onsala Space Observatory
Chalmers University of Technology
SE-412 96 Gothenburg
Sweden
Telephone: +46 (0)31-772 1000

Chalmers Reproservice
Gothenburg, Sweden 2023

The impact of loading-induced stress variation on the seismicity of active faults
YITING CAI
Department of Space, Earth and Environment
Chalmers University of Technology

Abstract

Surface loads such as the ocean, atmosphere, and continental water, constantly modify the stress field of the Earth's crust. Most earthquakes occur at tectonic plate boundaries and such stress perturbations on the active faults at the plate boundaries may trigger earthquakes. Several previous studies reported that tides or hydrological loading could modulate seismicity in some areas. We elaborate on this idea and further investigate the accumulative effect of various loadings.

In this work, we compute the total Coulomb stress change created by hydrological loading, atmospheric loading, and non-tidal ocean loading from 2011 to 2016 in the Kamchatka-Kuril Islands-Japan region, and then compare it to the background earthquakes in the same period. This thesis contributes to our understanding of the complex interactions between surface loading and induced seismicity, which has important implications for earthquake hazard assessment and risk mitigation.

Keywords: Seismicity, stress variation, Coulomb stress change, subduction zone

Acknowledgements

First and foremost, I would like to express my sincere gratitude to my supervisor Dr. Maxime Mouyen for his guidance, support, and mentorship throughout my studies. His expertise, encouragement, and constructive feedback have been invaluable in shaping my research and helping me grow as a researcher. I would also like to thank my cosupervisor, Dr. Karine le Bail, for her insightful comments, suggestions, and warm encouragement. I am grateful to my examiner Dr. Rüdiger Haas for his support, encouragement, and guidance.

My colleagues and fellow PhD students in the SEE department have been a constant source of inspiration and motivation, and I am grateful for their support and companionship.

Last but not the least, I would like to express my appreciation to my friends, partner, and family, who have always been there for me and provided me with their unconditional love and encouragement. Their belief in me has been my driving force. Their unwavering support has made this achievement possible.

Publications

This thesis is based on the work contained in the following papers:

I Y. Cai and M. Mouyen (2023). Loading-induced stress variation on active faults and seismicity modulation in the Kamchatka-Kuril Islands-Japan region. *Earth and Planetary Science Letters*. Submitted

Contents

Abstract i
Acknowledgements iii
Publications v
Contents vii

1 Introduction **1**
1.1 Outline of the thesis 2

2 Plate tectonics **3**
2.1 The lithosphere 4
2.2 Subduction zone 5
2.2.1 Slab2 6
2.3 Stress and the fault system 6

3 Non-tectonic modulation **11**
3.1 Non-tectonic stress variation 11
3.2 Stresses on the fault plane 13
3.3 Coulomb stress change 15

4 Background seismicity **17**
4.1 Sesmicity declustering 17
4.1.1 Gardner-Knopoff 18
4.1.2 Reasenberg 19
4.1.3 Other declustering algorithms 20
4.2 Magnitude of completeness 20

5 Summary and outlook **23**

Bibliography **25**

Paper I **29**

Chapter 1

Introduction

Throughout most of human history, people's understanding of earthquakes was dominated by mythology. For instance, in China, people believed that earthquakes were warnings and punishments from the gods due to distortions of the balance between *yin* and *yang*. In Greek mythology, *Poseidon*, the God of the Sea, was believed to show his rage by triggering earthquakes and tsunamis. These stories depict earthquakes as an unpredictable, uncontrollable, dramatic, and destructive phenomenon, which remains true based on our current knowledge of earthquakes. However, despite the advancement of modern technology and scientific progress, earthquakes are still not completely understood.

Destructive earthquakes can cause extensive damage and loss of life. According to data from the World Health Organization (WHO, 2023), between 1998 and 2017, earthquakes killed almost 750 000 people worldwide, which is more than half of all fatalities resulting from natural catastrophes in the same period. Earthquakes during this period had an impact on more than 125 million individuals. Earthquakes can also trigger other secondary hazards, such as soil liquefaction, landslides, avalanches, fires, and tsunamis. Therefore, earthquake research is important to reduce human vulnerability in front of the powerful nature. It is also an important part of sustainable development. For example, it can improve disaster preparedness and response, and contribute to better building codes and land use planning (Day, 2012). Also, earthquake research can help to promote sustainable economic development by reducing the costs of damage and disruption caused by earthquakes and improving the resilience of communities (Coburn and Spence, 2003). The recent progress in early warning systems can provide people with seconds or minutes to prepare for an earthquake and take necessary safety precautions (Allen and Melgar, 2019). In general, earthquake research is vital for our understanding of these natural disasters, their impact on society, and how we can prepare and respond to them.

Meanwhile, earthquake research can also help humans to understand the Earth better, especially its interior structure. To study such a big object like Earth, it is not feasible to have a direct observation of the interior as the depth increases. Earthquakes provide an indirect approach to the study of the physical features of

Earth, as seismic waves generated by earthquakes can provide information about the planet's internal structure (e.g. Karato and Karki, 2001; Stern, 2002). By studying earthquake behavior, researchers can better understand how they occur (e.g. Bouchon et al., 2013), how they propagate (e.g. Bray et al., 1994), how they affect the Earth's surface (e.g. Wesnousky, 2008) and the Earth's interior (e.g. Jamtveit et al., 2018).

Most earthquakes occur at tectonic plate boundaries, releasing part of the stress accumulated on faults by the continuous motion of the tectonic plates (e.g. Turcotte and Schubert, 2002). However, non-tectonic processes, such as tides and surface loading, can also build up stress on active faults. Tides and surface loads such as the atmosphere, sediment, continental water, or oceans continually generate elastic stresses in the Earth's lithosphere, and several studies have investigated the impact of such stress variations on seismicity in different geological settings all over the world, e.g. in California (Gao et al., 2000; Johnson et al., 2017), in Alaska (Johnson et al., 2020), in Missouri (Craig et al., 2017), in Japan (Heki, 2003), in Taiwan (Hsu et al., 2021), in the Himalayas (Bettinelli et al., 2008), and in Guerrero (Lowry, 2006). Most of the previous studies found a non-tectonic stress perturbation of a few kPa could modulate the seismicity, which indicates the local fault systems are critically stressed and sensitive to such small stress variation.

1.1 Outline of the thesis

The research of this thesis and the appended paper contribute to understanding earthquake nucleation by analyzing the stress variation induced by the non-tectonic processes on active faults in the subduction zone. This thesis aims to provide general background, introduce research tools and present some technical details. Chapter 2 introduces plate tectonics, the geometry model used in the study, and the relationship between stress and faults. Chapter 3 demonstrates an overview of the non-tectonic-loading-induced stress variation and how to evaluate its impact on active faults. Chapter 4 presents the necessary procedures for background seismicity analysis. Chapter 5 summarizes the thesis and the appended paper and also gives perspectives for future research.

Chapter 2

Plate tectonics

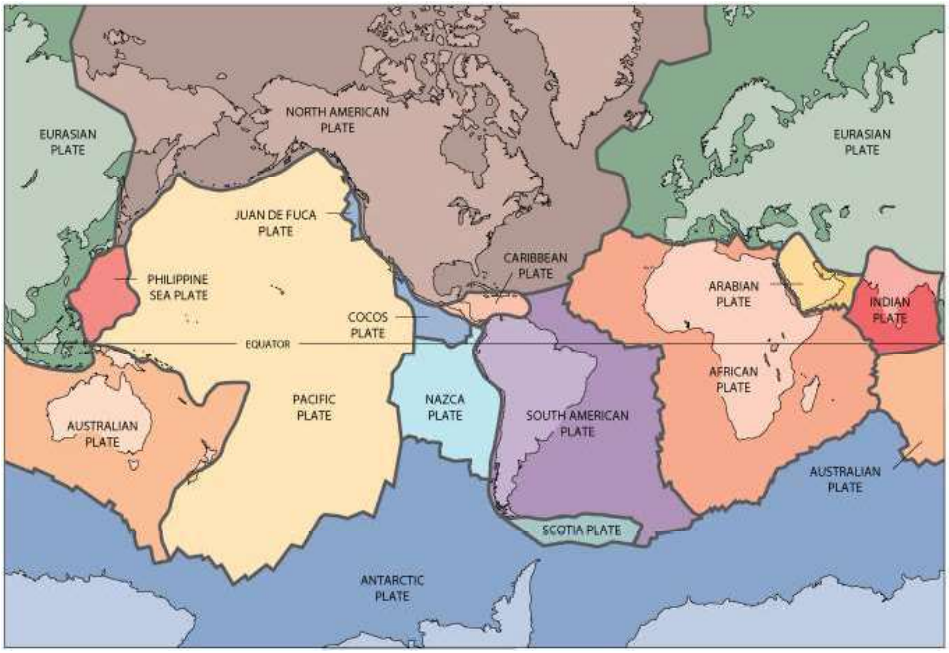

Figure 2.1: *The main tectonic plates and their boundaries* `https://pubs.usgs.gov/gip/dynamic/slabs.html`.

Plate tectonics[1] is a model that explains how the Earth's outer shell (lithosphere) is divided into a number of plates (see Figure 2.1) that move and interact with one another. These plates are composed of the Earth's crust and upper mantle, and they are constantly in motion due to the underlying convective movements

[1]This chapter is broadly based on Turcotte and Schubert, 2002, which serves as the general reference wherever other literature is not explicitly cited.

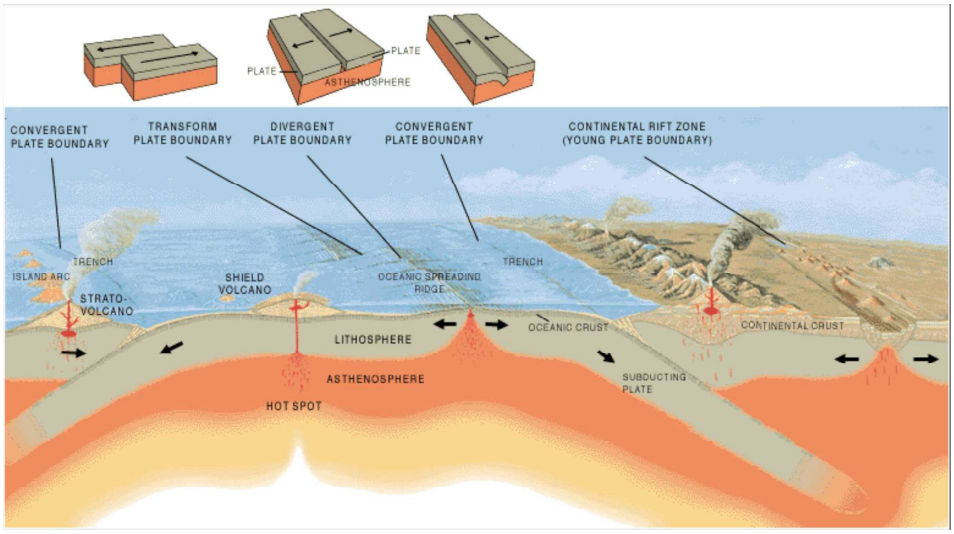

Figure 2.2: *The three main types of plate boundaries: divergent, convergent, and transform boundaries.* `https://www.usgs.gov/media/images/plate-boundary-types`.

in the mantle. The motion of these plates can cause a variety of geologic events, including earthquakes, volcanic eruptions, and the formation of mountains.

2.1 The lithosphere

The lithosphere is the outermost solid layer of the Earth, consisting of the crust and the uppermost part of the mantle. It is composed of a variety of different types of rocks, including basalt, granite, and sedimentary rocks, and is typically around 100 km thick beneath the oceans and doubles the thickness beneath the continents. The lithosphere is only 2 to 4% of the radius of the Earth and thus the lithosphere is a thin outer shell. The lithosphere plays a crucial role in shaping the surface features of the Earth, as well as in controlling the movement of heat and material between the planet's interior and exterior. The movement of the plates closely relates to earthquakes, especially at the plate boundaries.

There are three main types of plate boundaries (Figure 2.2), which are defined by the relative motion of the tectonic plates at each boundary. These three types of plate boundaries are divergent boundaries, convergent boundaries and transform boundaries. Divergent boundaries occur where two tectonic plates are moving away from each other. This type of boundary is usually found along mid-ocean ridges, e.g. the Mid-Atlantic Ridge, where new oceanic crust is formed as magma flows up from the mantle, cools, and solidifies. Convergent boundaries occur where two tectonic plates are moving toward each other. This type of boundary is usually associated with subduction zones, e.g. the Japan trench, where one plate is forced beneath the

other into the mantle. Convergent boundaries can also occur when two continental plates collide, resulting in the formation of mountain ranges. Transform boundaries occur where two tectonic plates are sliding past each other horizontally. This type of boundary is usually associated with fault zones, e.g. the San Andreas Fault in California. Transform boundaries can result in earthquakes as the plates move past each other, but they do not typically result in the formation or destruction of the crust.

2.2 Subduction zone

The subduction zone is associated with convergent boundaries. At the subduction zone, plates are colliding and one plate is being subducted beneath another. The plate that is being subducted typically consists of denser oceanic crust, while the overriding plate can be either the oceanic or continental crust. As the subducting plate descends into the mantle, it releases water and other volatiles, which can lead to the melting of the mantle rock above it, forming magma. This magma then rises to the surface and can result in volcanic activity. Subduction zones are also the location of many of the most powerful earthquakes, as the movement of the plates can result in the buildup of stress that is released in seismic activity. Figure 2.3 gives an example of subduction zone structure in northeastern Japan.

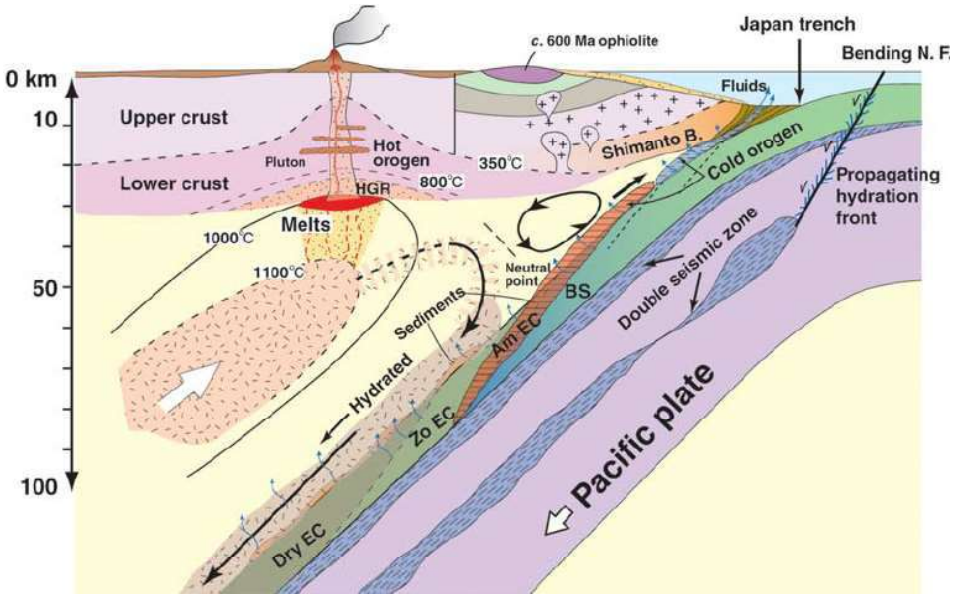

Figure 2.3: *The detailed sketch of the subduction zone structure of northeastern Japan (Santosh et al., 2010).*

2.2.1 Slab2

The Slab2 model (Hayes et al., 2018) is a comprehensive subduction zone geometry model that provides a detailed, three-dimensional representation of subducting plates. It covers an area of 24 million square kilometers and models slabs from the near-surface (oceanic trenches for most slabs) to their deepest expressions in the upper mantle. The model incorporates data from a variety of sources, including active-source seismic data interpretations, receiver functions, local and regional seismicity catalogs, and seismic tomography models. The subduction zone geometry model has a wide range of applications, from earthquake (e.g. Pagani et al., 2014) and tsunami (e.g. Geist and Lynett, 2014) hazard analyses to studies of mantle flow (e.g. Morishige and Honda, 2013). Slab2 is an important tool for advancing our understanding of subduction zones and the earthquakes that occur within them, and it is a valuable resource for researchers in the field of earth science.

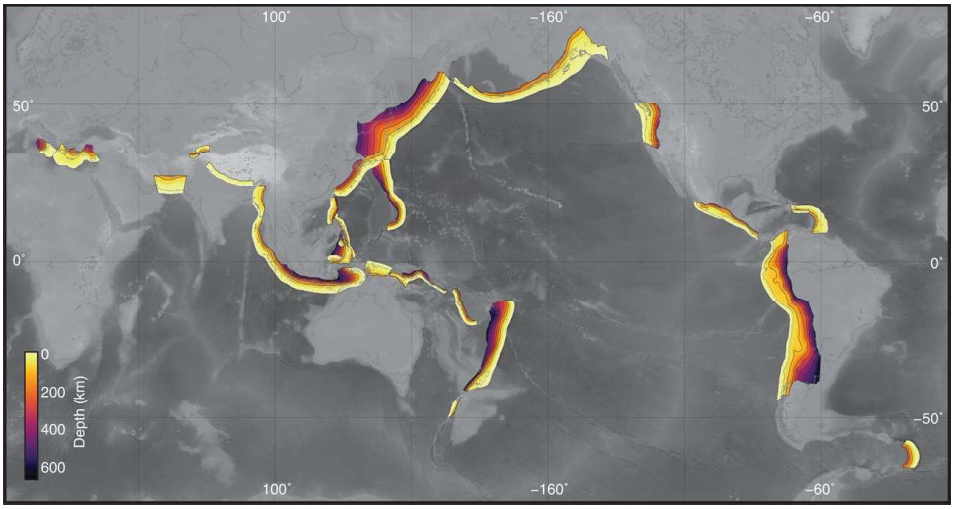

Figure 2.4: *The global distribution of models included in Slab2. Models are colored by depth (Hayes et al., 2018).*

2.3 Stress and the fault system

The earth's crust is under stress changes all the time (Figure 2.5), produced by both tectonic and non-tectonic processes. Studying the relationship between stress and the crust is important to understand the formation, evolution, deformation, and fracturing of the Earth's crust.

Principal stress Principal stress refers to the maximum and minimum stress that is acting on a point or region of rock. There are typically three principal stresses in any given region of rock, and they are referred to as the maximum

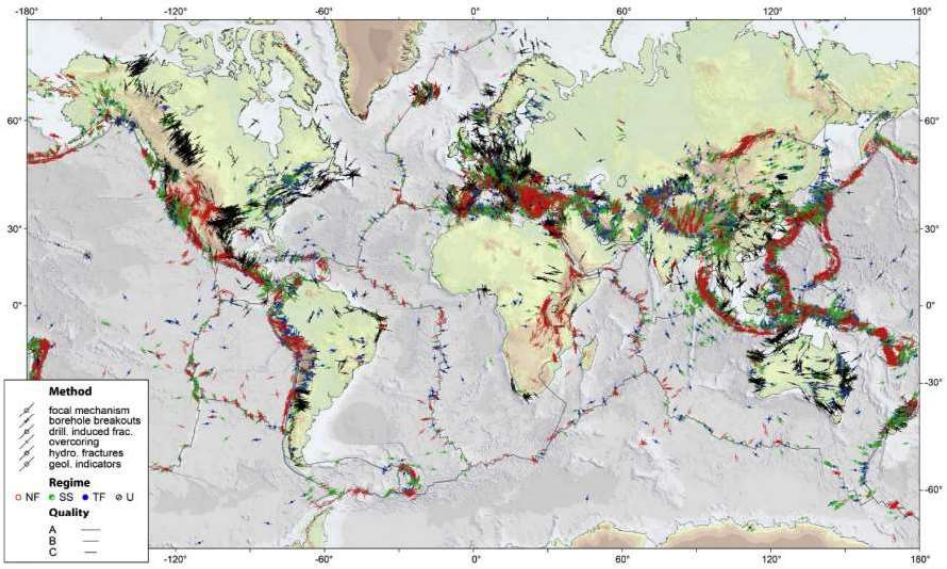

Figure 2.5: *World stress map 2016 (Heidbach et al., 2018). Lines indicate the orientation of maximum horizontal stress. The colors stand for the fault regime: red for normal faulting, green for strike-slip faulting, blue for thrust faulting, and black for the unknown regime. This map and the data set can be accessed and downloaded in high resolution at* `https://doi.org/10.5880/WSM.2016.002`.

principal stress σ_1, intermediate principal stress σ_2, and minimum principal stress σ_3. These principle stresses dictate how rocks will behave under stress and can influence factors such as the orientation of faults (Figure 2.6).

Strike-dip-rake Strike, dip, and rake are terms used to describe the orientation and direction of movement along a fault plane. As illustrated in Figure 2.7, strike refers to the direction of the line where the fault intersects the Earth's surface, while dip describes the angle of the fault plane relative to the horizontal. Rake is the direction of movement along the fault plane, measured in the horizontal plane and relative to the strike of the fault.

The stresses and the strike, dip, and rake of a fault are related, as the orientation and behavior of a fault will depend on the relative orientation of the applied stresses. For example, if the maximum principle stress is oriented perpendicular to the strike of a fault, it may be more likely to experience compression. Additionally, the orientation of the fault plane and its relationship to the stresses will influence the direction and amount of slip along the fault during an earthquake. Studying these relationships is important for understanding the behavior of faults and seismic activity in a given region.

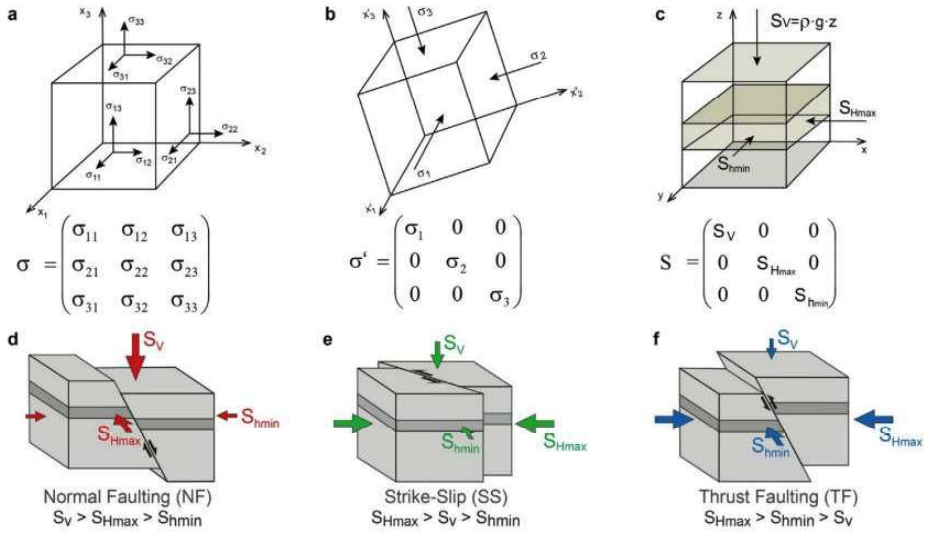

Figure 2.6: *Stress regime and fault kinematics (Heidbach et al., 2018). a) The components of the stress tensor define the stress state at a point and enable the computation of the stress vector on any surface within a body. b) The stress tensor has to be symmetric due to the conservation of momentum. c) The reduced stress tensor is determined with four components, the S_{Hmax} orientation and the magnitude of S_V, S_{Hmax}, and S_{Hmin}. d) Normal faulting. e) Strike-slip faulting. f) Thrust faulting.*

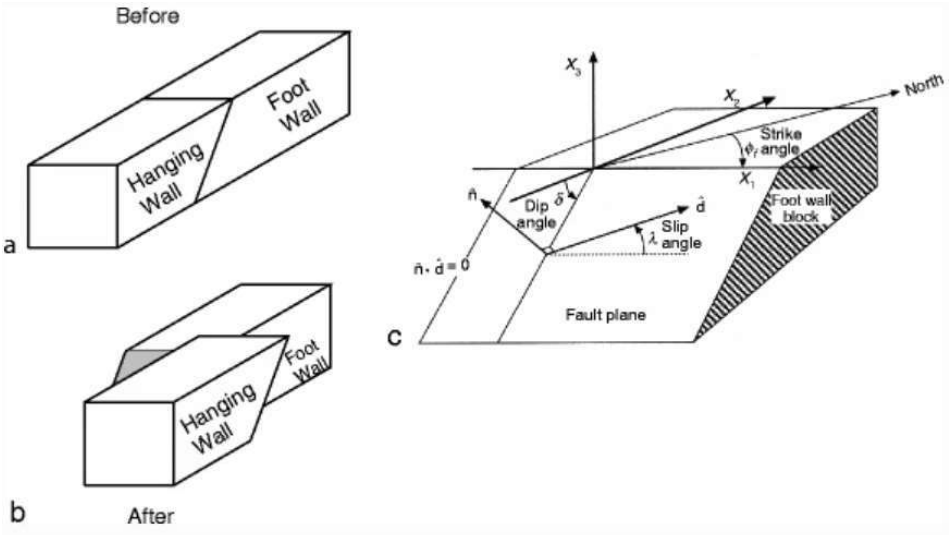

Figure 2.7: *a) and b) Before and after sketches of the displacement of fault blocks during an earthquake. The fault plane is shaded in b). c) Definition of the strike, dip, and rake angles, ϕ, δ, λ in the geometry of the rupture represented at left (Okal, 2011).*

Chapter 3

Non-tectonic modulation

Non-tectonic processes can induce stress changes that deform the Earth. These non-tectonic factors include hydrological loadings, atmospheric loading, ocean water, solid lunisolar tides, pole tides, and post-glacial rebound. These non-tectonic loading-induced stress changes have been found to modulate various tectonic events, including earthquakes (e.g. Craig et al., 2017), slow earthquakes (e.g. Liu et al., 2009), tremors (e.g. Nakata et al., 2008), slow slip events (e.g. Lowry, 2006), volcanoes (e.g. Kasahara, 2002), and landslides (e.g. Tsou et al., 2011).

To investigate the non-tectonic modulation of earthquakes, one approach is to compute Coulomb stress change (ΔCFF) induced by the non-tectonic loadings and to evaluate if they correlate with the variations of seismicity. Computing Coulomb stress change requires two pieces of information: 1) the fault parameters and 2) the values of stresses applied to the fault, specifically the shear stress and the normal stress, which will be described in Section 3.3 The former information is given in the Slab2 subduction zone geometry model (see section 2.2). This chapter first introduces the non-tectonic loadings and their induced stress variation, then describes the procedure we applied in the study to calculate the normal and shear stresses on the fault and further the Coulomb stress change.

3.1 Non-tectonic stress variation

The Earth responds to non-tectonic processes in both elastic and viscoelastic ways, depending on the Earth's layers they affect. Tides and surface loads such as the atmosphere, sediment, continental water, or oceans continually generate elastic stresses in the Earth's lithosphere in a short time scale of a few hours to a few years. While the Earth responds in a viscoelastic way to the surface glacial loading of a much longer time scale. Figure 3.1 sketch these two types of loadings and the Earth's corresponding responses.

The elastic stress variations, given in Lu et al., 2018, are derived with a compressible and elastic Gutenberg-Bullen A Earth model, and the strain-stress relation given in Equation 3.1, where λ and μ are the Lamé constants and δ_{ij} is the Kronecker delta. For the viscoelastic stress variations, Lu et al., 2018 adopt a

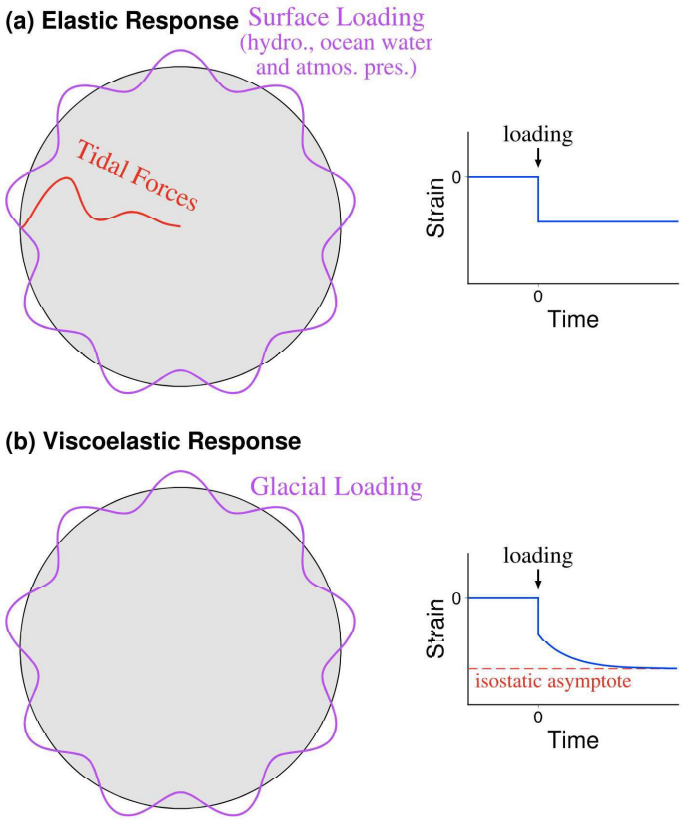

Figure 3.1: *Sketch loading forces and the Earth's respective a) elastic and b) viscoelastic responses Lu et al., 2018.*

constitutive relationship of an incompressible Maxwell viscoelastic body, as shown in Equation 3.2, where η is viscosity, P is pressure and the dot is time derivative. More details of the theory, data sources, and computation are given in Lu et al., 2018, references therein, and the corresponding database.

$$\sigma_{ij} = \lambda \varepsilon_{kk} \delta_{ij} + 2\mu \varepsilon_{ij} \tag{3.1}$$

$$\sigma_{ij} + \frac{\eta}{\mu} \dot{\sigma}_{ij} = -(P + \frac{\eta}{\mu} \dot{P}) \delta_{ij} + 2\eta \dot{\varepsilon}_{ij} \tag{3.2}$$

The non-tectonic-loading-induced stress variations are given as stress tensors with six independent components in the $r - \theta - \phi$ (radius-longitude-colatitude) geographic reference system on $1^\circ \times 1^\circ$. Table 3.1 gives an overview of the maximum amplitude of the four surface deviatoric stress components induced by different loadings.

load	S_{rr} [bar]	$S_{\theta\theta}$ [bar]	$S_{\phi\phi}$ [bar]	$S_{\theta\phi}$ [bar]
Hydrological loading	4.3×10^{-2}	2.1×10^{-2}	2.3×10^{-2}	3.8×10^{-2}
Atmosphere pressure	1.6×10^{-2}	8.7×10^{-3}	7.9×10^{-3}	2.7×10^{-3}
Ocean tide	7.8×10^{-1}	3.8×10^{-1}	4.1×10^{-1}	2.3×10^{-1}
Non-tidal ocean	5.7×10^{-2}	3.7×10^{-2}	3.6×10^{-2}	2.2×10^{-2}
Solid lunisolar tide	4.1×10^{-2}	2.5×10^{-2}	2.2×10^{-2}	1.7×10^{-2}
Pole tide	1.1×10^{-3}	3.2×10^{-4}	7.8×10^{-4}	4.5×10^{-5}
Post-glacial rebound [1]	1.6×10^{-2}	8.7×10^{-2}	8.0×10^{-2}	2.9×10^{-2}

Table 3.1: Maximum amplitudes of the four surface deviatoric stress components caused by the different loading forces, between 2000 and 2017 (Lu et al., 2018).

3.2 Stresses on the fault plane

With the stress variations generated as described above, we now can move forward to the next step of Coulomb stress change computation, i.e. computing the normal stress and the shear stress on the fault plane. Our computation consists of three steps, 1) transforming the stress tensor, 2) defining the fault plane coordinate system, and 3) decomposing the stress tensor in the geographical coordinate system onto the fault base vectors.

We transform the stress tensor given in the $r-\theta-\phi$ (radius-longitude-colatitude) coordinate system to the N-E-D (North-East-Down) coordinate system. Both are right-handed systems. The stress tensor $\underline{\underline{T}}$ is a second-order tensor consisting of nine components T_{ij} that completely define the state of stress. There are six independent components because the stress tensor must be a symmetric matrix constrained by the conservation of momentum.

$$\underline{\underline{T}}_{r\theta\phi} = \begin{bmatrix} T_{rr} & T_{\theta r} & T_{\phi r} \\ T_{r\theta} & T_{\theta\theta} & T_{\phi\theta} \\ T_{r\phi} & T_{\theta\phi} & T_{\phi\phi} \end{bmatrix} \tag{3.3}$$

$$\underline{\underline{T}}_{NED} = \begin{bmatrix} T_{NN} & T_{EN} & T_{DN} \\ T_{NE} & T_{EE} & T_{DE} \\ T_{ND} & T_{ED} & T_{DD} \end{bmatrix} = \begin{bmatrix} T_{\theta\theta} & -T_{\theta\phi} & T_{r\theta} \\ -T_{\theta\phi} & T_{\phi\phi} & -T_{r\phi} \\ T_{r\theta} & -T_{r\phi} & T_{rr} \end{bmatrix} \tag{3.4}$$

The basis vectors are notated as $(\hat{r}, \hat{\theta}, \hat{\phi})$ and $(\hat{N}, \hat{E}, \hat{D})$ for the $r-\theta-\phi$ coordinate system and the N-E-D coordinate system, respectively. The relationship between the two sets of basis vectors is shown in Equation 3.5. By substituting Equation 3.5 into the derivation procedure, we give the tensor transformation from the tensor operator perspective in Equation 3.6. Note that the stress convention in the original database Lu et al., 2018 is positive for extension and negative for compression. We alter the sign of each component to fit the stress tensor into the desired convention for further computation, where positive stands for compression and negative stands for tension.

$$\hat{N} = -\hat{\theta}, \hat{E} = \hat{\phi}, \hat{D} = -\hat{r} \tag{3.5}$$

$$\begin{aligned}
\underline{\underline{T}}_{NED} = & \quad \hat{N}T_{NN}\hat{N}\cdot + \hat{E}T_{EN}\hat{N}\cdot + \hat{D}T_{DN}\hat{N}\cdot \\
& + \hat{N}T_{NE}\hat{E}\cdot + \hat{E}T_{EE}\hat{E}\cdot + \hat{D}T_{DE}\hat{E}\cdot \\
& + \hat{N}T_{ND}\hat{D}\cdot + \hat{E}T_{ED}\hat{D}\cdot + \hat{D}T_{DD}\hat{D}\cdot \\
= & \quad \hat{r}T_{rr}\hat{r}\cdot + \hat{\theta}T_{\theta r}\hat{r}\cdot + \hat{\phi}T_{\phi r}\hat{r}\cdot \\
& + \hat{r}T_{r\theta}\hat{\theta}\cdot + \hat{\theta}T_{\theta\theta}\hat{\theta}\cdot + \hat{\phi}T_{\phi\theta}\hat{\theta}\cdot \\
& + \hat{r}T_{r\phi}\hat{\phi}\cdot + \hat{\theta}T_{\theta\phi}\hat{\phi}\cdot + \hat{\phi}T_{\phi\phi}\hat{\phi}\cdot \\
= & \quad (-\hat{D})T_{rr}(-\hat{D})\cdot + (-\hat{N})T_{\theta r}(-\hat{D})\cdot + (+\hat{E})T_{\phi r}(-\hat{D})\cdot \\
& + (-\hat{D})T_{r\theta}(-\hat{N})\cdot + (-\hat{N})T_{\theta\theta}(-\hat{N})\cdot + (+\hat{E})T_{\phi\theta}(-\hat{N})\cdot \\
& + (-\hat{D})T_{r\phi}(+\hat{E})\cdot + (-\hat{N})T_{\theta\phi}(+\hat{E})\cdot + (+\hat{E})T_{r\phi}(+\hat{E})\cdot \\
= & \quad \hat{D}(+T_{rr})\hat{D}\cdot + \hat{N}(+T_{\theta r})\hat{D}\cdot + \hat{E}(-T_{\phi r})\hat{D}\cdot \\
& + \hat{D}(+T_{r\theta})\hat{N}\cdot + \hat{N}(+T_{\theta\theta})\hat{N}\cdot + \hat{E}(-T_{\phi\theta})\hat{N}\cdot \\
& + \hat{D}(-T_{r\phi})\hat{E}\cdot + \hat{N}(-T_{\theta\phi})\hat{E}\cdot + \hat{E}(+T_{r\phi})\hat{E}\cdot \\
= & \quad \hat{N}(+T_{\theta\theta})\hat{N}\cdot + \hat{E}(-T_{\phi\theta})\hat{N}\cdot + \hat{D}(+T_{r\theta})\hat{N}\cdot \\
& + \hat{N}(-T_{\theta\phi})\hat{E}\cdot + \hat{E}(+T_{r\phi})\hat{E}\cdot + \hat{D}(-T_{r\phi})\hat{E}\cdot \\
& + \hat{N}(+T_{\theta r})\hat{D}\cdot + \hat{E}(-T_{\phi r})\hat{D}\cdot + \hat{D}(+T_{rr})\hat{D}\cdot
\end{aligned} \tag{3.6}$$

The next step is defining the fault plane coordinate system d-s-n (dip-strike-normal). The basis consists of three vectors: $\underline{n}_d$ (dip), $\underline{n}_s$ (strike), and $\underline{n}_n$ (normal), defined by Equation 3.7, 3.8 and 3.9, respectively. The fault plane is illustrated in Figure 3.2.

$$\underline{n}_d = \begin{bmatrix} -\sin(strike)\cos(dip) \\ \cos(strike)\cos(dip) \\ -\sin(dip) \end{bmatrix} \tag{3.7}$$

$$\underline{n}_s = \begin{bmatrix} \cos(strike) \\ \sin(strike) \\ 0 \end{bmatrix} \tag{3.8}$$

$$\underline{n}_n = \begin{bmatrix} -\sin(strike)\sin(dip) \\ \cos(strike)\sin(dip) \\ -\cos(dip) \end{bmatrix} \tag{3.9}$$

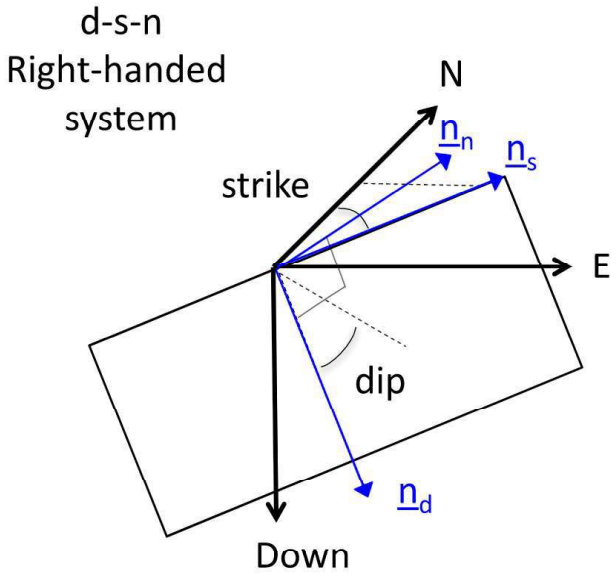

Figure 3.2: *Fault coordinate system as a function of strike and dip.*

The last step is to project the stress tensor based on the N-E-D (North-East-Down) geographical coordinate system onto the fault base vectors. The stress vector acting on the fault $\underline{t}$ is calculated as in Equation 3.10. The total normal stress on the fault plane σ_n is defined by Equation 3.11, which is aligned with $\underline{n}_n$. After obtaining $\underline{t}$ and σ_n, the apparent shear stress τ_a therefore can be calculated according to Equation 3.12.

$$\underline{t} = \underline{\underline{T}}_{NED}\underline{n}_n \tag{3.10}$$

$$\sigma_n = \underline{t} \cdot \underline{n}_n \tag{3.11}$$

$$\tau_a = \sqrt{||\underline{t}||^2 - ||\underline{t} \cdot \underline{n}_n||^2} \tag{3.12}$$

3.3 Coulomb stress change

The Coulomb stress change (ΔCFF) quantifies whether a fault is getting closer ($\Delta CFF > 0$) to or further ($\Delta CFF < 0$) from rupture when subjected to a given

stress condition (King et al., 1994). The greater normal stress σ_n leads to lower ΔCFF, assuming the shear stress stays the same. With compression given as positive values, the physics behind is that the fault is more loaded and locked and therefore tends to clamp. The Coulomb stress change ΔCFF is defined as:

$$\Delta CFF = \Delta\tau - \mu(\Delta\sigma_n - \Delta p) \tag{3.13}$$

where the terms $\Delta\tau$ stands for the shear stress change aligned in the fault rake direction, $\Delta\sigma_n$ represent the changes in the normal stress on the fault, μ is the friction coefficient and Δp is the change in pore pressure in the fault zone. Assuming that the change in pore pressure Δp is proportional to σ_n (Cocco and Rice, 2002), we can introduce the effective friction coefficient μ' (King et al., 1994) to obtain ΔCFF according to the formula in Equation 3.14, where $\mu' = \mu(1 - B)$ and B is the Skempton coefficient.

$$\Delta CFF = \Delta\tau - \mu'\Delta\sigma_n \tag{3.14}$$

It is worth noting that the shear stress τ in this section is not the same as the apparent shear stress τ_a in Equation 3.12 in the last section. τ is the projection of τ_a onto the fault rake direction.

$$\begin{aligned} \tau &= \tau_a * \cos(rake_{stress} - rake_{fault}) \\ &= \tau_a * \cos(\arctan(\frac{\underline{t} \cdot \underline{n}_d}{\underline{t} \cdot \underline{n}_s}) - rake_{fault}) \end{aligned} \tag{3.15}$$

Chapter 4

Background seismicity

Several thousands of globally distributed seismic stations maintained by many different agencies allow researchers to monitor and record the seismicity on Earth with unprecedented accuracy. Services such as the ISC (International Seismological Centre) or the USGS (United States Geological Survey) report comprehensive earthquake catalogs that serve numerous applications related to earthquake science. Among these earthquakes, one can distinguish independent earthquakes and clustered earthquakes.

The clustered seismicity is mostly considered as tectonic driven. For example, aftershocks are usually assumed to be triggered by dynamic or static stress changes imposed by the mainshocks (Stein, 1999; Toda et al., 2012), and earthquake swarms are thought to result from underlying crustal transient processes (Chen et al., 2012). Thus, it is important to have catalogs that only consist of independent earthquakes and exclude clear forms of clustered events to analyze non-tectonic seismicity modulation.

The process of separating earthquakes into independent and dependent classes is known as seismicity declustering. Declustering algorithms aim to divide the catalog into independent earthquakes (mainshocks and single events) and clusters with dependent events (such as aftershocks). With the result from the declustering process, we can then remove spatiotemporal densely clustered events and minimize the dependency among the seismic activities.

Many declustering algorithms exist. We will introduce the window method and the linked-window method and also mention other algorithms in this chapter[1]. We then will also describe the concept of the magnitude of completeness and why it is important for seismicity analysis.

4.1 Sesmicity declustering

To distinguish independent mainshocks from the catalog, the declustering algorithm must first define a conceptual model of what is a mainshock. Due to the complexity

[1]This chapter is broadly based on Stiphout et al., 2012 and Mignan and Woessner, 2012, which serve as the general reference wherever other literature is not explicitly cited.

M	d(M) [km]	t(M) [days]
2.5	19.5	6
3.0	22.5	11.5
3.5	26	22
4.0	30	42
4.5	35	83
5.0	40	155
5.5	47	290
6.0	54	510
6.5	61	790
7.0	70	915
7.5	81	960
8.0	94	985

Table 4.1: Windows for identifying aftershocks (Gardner and Knopoff, 1974).

of earthquakes, this underlying model differs from one algorithm to another and there is no absolutely best algorithm. Here we introduce two types of existing methods that are used in our study, which are the Gardner-Knopoff algorithm and the Reasenberg algorithm. The implementation of these algorithms is available in the MATLAB tool for seismicity analysis, ZMAP (Wiemer, 2001).

4.1.1 Gardner-Knopoff

The Gardner-Knopoff (G-K) algorithm is also known as the window method because it provides a specific space-time window as a function of the mainshock magnitude to identify aftershocks. This algorithm was introduced by Gardner and Knopoff, 1974 and the original identification windows provided by the authors are given as Table 4.1. These windows give the space and time proximity of the earthquakes depending on the mainshocks. For each earthquake in the catalog with magnitude M, the subsequent shocks are identified as aftershocks if they occur within a specified time interval t(M), and a distance interval d(M). Equation 4.1 displays an approximation of the corresponding window size. These parameters were derived in the 1970s from the earthquakes in Southern California, and it was encouraged to try out other values for other areas and periods. Later in 1986, another set of window parameters (Equation 4.2) of the G-K algorithm was proposed by Uhrhammer, 1986 and it's also widely used by research nowadays.

Original window

$$
\begin{aligned}
d &= e^{0.1238*M+0.983} \quad [km] \\
t &= \begin{cases} |10^{0.032*M+2.7389}|, & \text{if M} \geq 6.5 \\ 10^{0.5409*M-0.547}, & \text{if M} < 6.5 \end{cases} \quad [days]
\end{aligned} \tag{4.1}
$$

Uhrhammer window

$$d = e^{1.77+(0.037+1.02*M)^2} \quad [km]$$
$$t = \begin{cases} |e^{-3.95+(0.62+17.32*M)^2}|, & \text{if M} \geq 6.5 \\ 10^{2.8+0.024*M}, & \text{if M} < 6.5 \end{cases} \quad [days] \tag{4.2}$$

4.1.2 Reasenberg

Reasenberg algorithm is a linked-window method, which links earthquakes to clusters according to spatial and temporal interaction zones. The spatial extension of the interaction zone is $\log d = 0.4M - 1.943 + k[km]$ (Molchan and Dmitrieva, 1992), k is 1 for proximity to the largest event and 0 for proximity to the last one. The temporal extension of the interaction zone is based on Omori's law (Omori, 1895) that the rate of aftershocks is proportional to the inverse of time, i.e. the amount of time required to wait for the subsequent aftershock grows proportionally as the time from the mainshock increases.

The standard parameters in Table 4.2 were derived for Northern California (Reasenberg, 1985). τ_{min} and τ_{max} are the minimum and maximum values of the look-ahead time for building clusters when the first event is not clustered. p_1 is the probability of detecting the next clustered event used to compute the look-ahead time τ. x_k is the increase of the lower cut-off magnitude during clusters. x_{meff} is the effective lower magnitude cutoff for the catalog. During clusters, x_{meff} is raised by a factor x_k of the magnitude M of the largest earthquake in the cluster: $x_{meff} = x_{meff} + x_k M$. r_{fact} is the number of crack radii (Kanamori and Anderson, 1975) surrounding each earthquake within new events considered to be part of the cluster. The relationship of the parameters is displayed as the formulae in Equation 4.3, where $\Delta M = M_{mainshock} - x_{meff}$.

$$\tau = \frac{-\ln(1-p_1)t}{10^{2(\Delta M-1)/3}} \tag{4.3}$$

Parameter	τ_{min} [days]	τ_{max} [days]	p_1	x_k	x_{meff}	r_{fact}
Standard value	1	10	0.95	0.5	1.5	10

Table 4.2: Input parameters for Reasenberg declustering algorithm (Reasenberg, 1985), derived for north Carlifornia. Parameters are described in the texts.

In this work, all the aforementioned algorithms and windows are tested to decluster the catalog, and the temporal distribution of the cumulative events can be found in Figure 4.1. The noticeable climbing earthquake number in March 2011 because of the aftershocks of the M_W 9.1 Tohuku earthquake is suppressed by the declustering process.

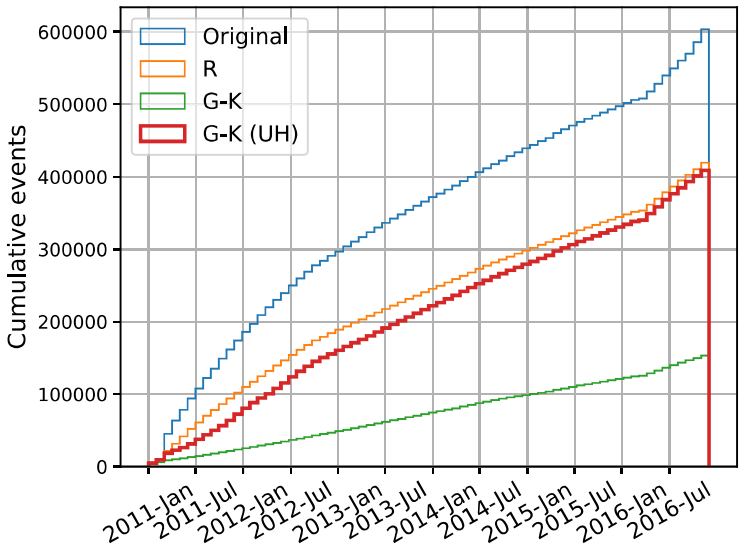

Figure 4.1: *The cumulative seismicity of the original catalog and the declustered catalogs. R: Reasenberg algorithm with the standard parameters (Reasenberg, 1985), G-K: Gardner-Kopnoff algorithm with the original window (Gardner and Knopoff, 1974), G-K (UH): Gardner-Kopnoff algorithm with the Uhrhammer window Uhrhammer, 1986.*

4.1.3 Other declustering algorithms

Both the Gardner-Knopoff algorithm and the Reasenberg algorithm are deterministic and involve subjective parameter-choosing procedures. There are also many other stochastic declustering algorithms developed over the years, e.g. the stochastic declustering with Epidemic Type Aftershock Sequence (ETAS) model (Zhuang et al., 2002) and the Model-Independent Stochastic Declustering (MISD) (Marsan and Lengline, 2008). More details about these methods can be found in the review by Stiphout et al., 2012.

4.2 Magnitude of completeness

Another important step in seismicity analysis is to assess the magnitude of completeness Mc, which is defined as the lowest magnitude at which 100% of the earthquakes in a space-time volume are detected. For example, if the Mc of a catalog is 1.0, this means that all earthquakes above a magnitude 1.0 have been recorded in the catalog.

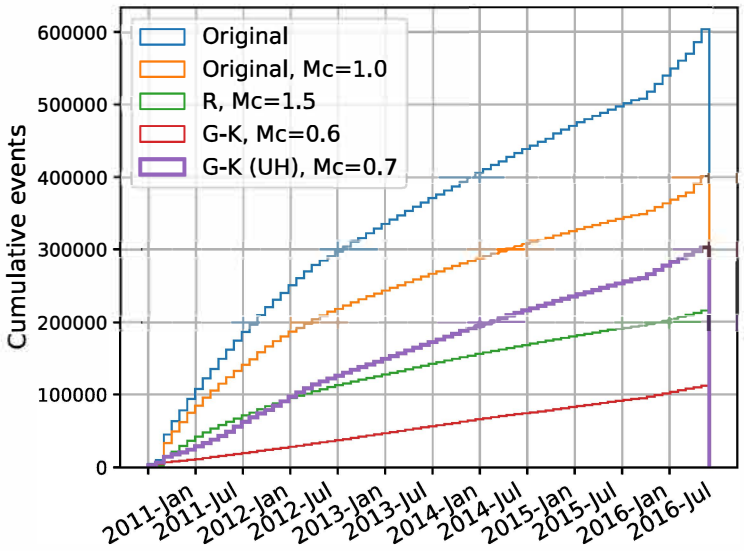

Figure 4.2: *Same as Figure 4.1 except with the magnitude of completeness Mc cutoff, i.e. removing the events with a magnitude below Mc.*

The magnitude of completeness (Mc) is estimated by fitting a Gutenberg-Richter (G-R) model (Gutenberg and Richter, 1944) to the observed frequency-magnitude distribution (FMD).

$$log_{10}N = a - b(m - M_c) \tag{4.4}$$

where Mc is the magnitude at which the lower end of the FMD departs from the G-R law, N is the number of events with magnitude greater or equal to m, a is the earthquake productivity and b describes the relative distribution of small and large earthquakes. The choice of the minimum magnitude cutoff Mc can influence the overall seismicity rate by affecting the b and a values. One can see the influence of Mc cutoff on the seismicity rate by comparing Figure 4.2 to Figure 4.1.

The example frequency-magnitude distribution (FMD) plot of the catalog used in our study declustered with Gardner-Knopoff algorithm, Uhrhammer window, is as Figure 4.3. The magnitude of completeness (Mc) is marked by a blue triangle in each plot. Mc is determined by the Maximum Curvature (MAXC) method (Wiemer and Wyss, 2000) that consists in defining the point of the maximum curvature by computing the maximum value of the first derivative of the frequency-magnitude curve.

In summary, the impact of declustering methods and the magnitude of completeness cutoff on the spatiotemporal distribution of background seismicity is shown in Figure 4.2, which can affect the results when comparing seismicity to stress variations. To maximize the background earthquake numbers while suppressing the impact of major earthquakes in the region, we chose the Gardner and Knopoff

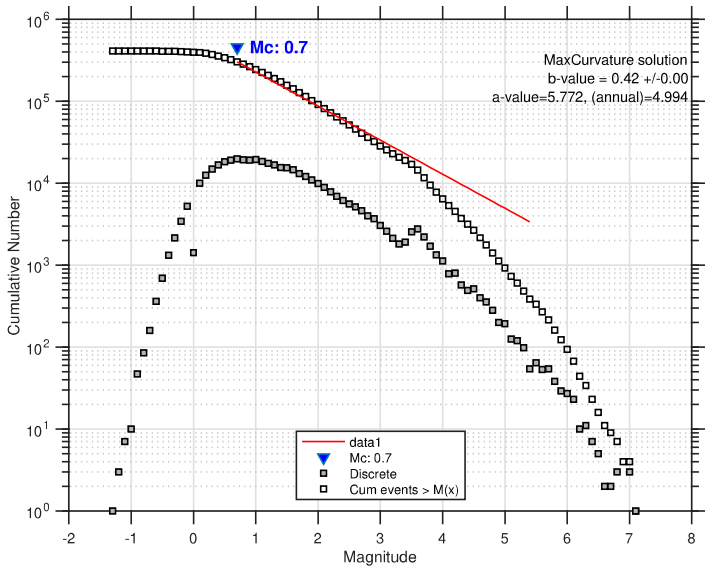

Figure 4.3: *FMD plot of the catalog declustered by the Gardner-Knopoff algorithm with the window defined by Uhrhammer, Mc=0.7*

algorithm with the Uhrhammer window in our study.

Chapter 5

Summary and outlook

Summary of Paper I

In this paper, we examine the relationship between stress variations due to surface loadings, including hydrological, atmospheric, and non-tidal ocean loading, and the earthquake that occurred in the subduction zone in the Kamchatka-Kuril Islands-Japan region between 2011 and 2016. We observed a positive correlation between earthquake occurrence and the stress variation induced by surface loading from non-tectonic processes. The loading-induced Coulomb stress changes of only a few kPa are sufficient to weakly modulate the earthquakes in the shallow portion of the Japan trench and Kuril trench, which indicates the local faults are critically stressed. Our results show the primary loading, which contributes the most to the loading-induced Coulomb stress change, varies across the studied area and varies the spatiotemporal distribution of the Coulomb stress change. Such variability suggests the importance of the accumulation of different loading sources in the loading-induced seismicity analysis.

Outlook

The research presented in this thesis and the accompanying paper make significant contributions to our understanding of the loading-induced seismicity along the Japan Trench and the Kuril Trench between 2011 and 2016. To continue building on the findings of this study, there are several directions for future research. One is to investigate not only the accumulated loading sources but also the accumulated stress period, and then examine the relationship between the stressing duration and the earthquake occurrence. Also, assessing the shear stress, normal stress, and principal stresses in relation to earthquake activities can provide valuable insights. Another direction is including more stress sources such as tidal stress, which can expand the stress budget and contribute to a more comprehensive understanding of seismicity nucleation. Additionally, there is potential to apply the methods and techniques used in this study to other regions, other periods, or other types of seismic activity, to further advance the field of seismicity research.

Bibliography

Allen, R. M. and D. Melgar (2019). Earthquake early warning: Advances, scientific challenges, and societal needs. *Annual Review of Earth and Planetary Sciences*, **47**, 361–388.

Bettinelli, P., J.-P. Avouac, M. Flouzat, L. Bollinger, G. Ramillien, S. Rajaure, and S. Sapkota (2008). Seasonal variations of seismicity and geodetic strain in the Himalaya induced by surface hydrology. *Earth and Planetary Science Letters*, **266**(3-4), 332–344.

Bouchon, M., V. Durand, D. Marsan, H. Karabulut, and J. Schmittbuhl (2013). The long precursory phase of most large interplate earthquakes. *Nature geoscience*, **6**(4), 299–302.

Bray, J. D., R. B. Seed, L. S. Cluff, and H. B. Seed (1994). Earthquake fault rupture propagation through soil. *Journal of Geotechnical Engineering*, **120**(3), 543–561.

Cai, Y. and M. Mouyen (2023). Loading-induced stress variation on active faults and seismicity modulation in the Kamchatka-Kuril Islands-Japan region. *Earth and Planetary Science Letters*. Submitted.

Chen, X., P. Shearer, and R. Abercrombie (2012). Spatial migration of earthquakes within seismic clusters in Southern California: Evidence for fluid diffusion. *Journal of Geophysical Research: Solid Earth*, **117**(B4).

Coburn, A. and R. Spence (2003). *Earthquake protection*. John Wiley & Sons.

Cocco, M. and J. R. Rice (2002). Pore pressure and poroelasticity effects in Coulomb stress analysis of earthquake interactions. *Journal of Geophysical Research: Solid Earth*, **107**(B2), ESE–2.

Craig, T. J., K. Chanard, and E. Calais (2017). Hydrologically-driven crustal stresses and seismicity in the New Madrid Seismic Zone. *Nature communications*, **8**(1), 2143.

Day, R. W. (2012). *Geotechnical earthquake engineering handbook: with the 2012 International building code*. McGraw-Hill Education.

Gao, S. S., P. G. Silver, A. T. Linde, and I. S. Sacks (2000). Annual modulation of triggered seismicity following the 1992 Landers earthquake in California. *Nature*, **406**(6795), 500–504.

Gardner, J. and L. Knopoff (1974). Is the sequence of earthquakes in Southern California, with aftershocks removed, Poissonian? *Bulletin of the seismological society of America*, **64**(5), 1363–1367.

Geist, E. L. and P. J. Lynett (2014). Source processes for the probabilistic assessment of tsunami hazards. *Oceanography*, **27**(2), 86–93.

Gutenberg, B. and C. F. Richter (1944). Frequency of earthquakes in California. *Bulletin of the Seismological society of America*, **34**(4), 185–188.

Hayes, G. P., G. L. Moore, D. E. Portner, M. Hearne, H. Flamme, M. Furtney, and G. M. Smoczyk (2018). Slab2, a comprehensive subduction zone geometry model. *Science*, **362**(6410), 58–61.

Heidbach, O., M. Rajabi, X. Cui, K. Fuchs, B. Müller, J. Reinecker, K. Reiter, M. Tingay, F. Wenzel, F. Xie, et al. (2018). The World Stress Map database release 2016: Crustal stress pattern across scales. *Tectonophysics*, **744**, 484–498.

Heki, K. (2003). Snow load and seasonal variation of earthquake occurrence in Japan. *Earth and Planetary Science Letters*, **207**(1-4), 159–164.

Hsu, Y.-J., H. Kao, R. Bürgmann, Y.-T. Lee, H.-H. Huang, Y.-F. Hsu, Y.-M. Wu, and J. Zhuang (2021). Synchronized and asynchronous modulation of seismicity by hydrological loading: A case study in Taiwan. *Science Advances*, **7**(16), eabf7282.

Jamtveit, B., Y. Ben-Zion, F. Renard, and H. Austrheim (2018). Earthquake-induced transformation of the lower crust. *Nature*, **556**(7702), 487–491.

Johnson, C. W., Y. Fu, and R. Bürgmann (2017). Seasonal water storage, stress modulation, and California seismicity. *Science*, **356**(6343), 1161–1164.

— (2020). Hydrospheric modulation of stress and seismicity on shallow faults in southern Alaska. *Earth and Planetary Science Letters*, **530**, 115904.

Kanamori, H. and D. L. Anderson (1975). Theoretical basis of some empirical relations in seismology. *Bulletin of the seismological society of America*, **65**(5), 1073–1095.

Karato, S.-i. and B. B. Karki (2001). Origin of lateral variation of seismic wave velocities and density in the deep mantle. *Journal of Geophysical Research: Solid Earth*, **106**(B10), 21771–21783.

Kasahara, J. (2002). Tides, earthquakes, and volcanoes. *Science*, **297**(5580), 348–349.

King, G. C., R. S. Stein, and J. Lin (1994). Static stress changes and the triggering of earthquakes. *Bulletin of the Seismological Society of America*, **84**(3), 935–953.

Liu, C., A. T. Linde, and I. S. Sacks (2009). Slow earthquakes triggered by typhoons. *Nature*, **459**(7248), 833–836.

Lowry, A. R. (2006). Resonant slow fault slip in subduction zones forced by climatic load stress. *Nature*, **442**(7104), 802–805.

Lu, Z., H. Yi, and L. Wen (2018). Loading-induced Earth's stress change over time. *Journal of Geophysical Research: Solid Earth*, **123**(5), 4285–4306.

Marsan, D. and O. Lengline (2008). Extending earthquakes' reach through cascading. *Science*, **319**(5866), 1076–1079.

Mignan, A. and J. Woessner (2012). Estimating the magnitude of completeness for earthquake catalogs. *Community Online Resource for Statistical Seismicity Analysis*, 1–45.

Molchan, G. and O. Dmitrieva (1992). Aftershock identification: methods and new approaches. *Geophysical Journal International*, **109**(3), 501–516.

Morishige, M. and S. Honda (2013). Mantle flow and deformation of subducting slab at a plate junction. *Earth and Planetary Science Letters*, **365**, 132–142.

Nakata, R., N. Suda, and H. Tsuruoka (2008). Non-volcanic tremor resulting from the combined effect of Earth tides and slow slip events. *Nature Geoscience*, **1**(10), 676–678.

Okal, E. A. (2011). *Earthquake, Focal Mechanism*. Encyclopedia of Solid Earth Geophysics. Springer.

Omori, F. (1895). "On the after-shocks of earthquakes". PhD thesis. The University of Tokyo.

Pagani, M., D. Monelli, G. Weatherill, L. Danciu, H. Crowley, V. Silva, P. Henshaw, L. Butler, M. Nastasi, L. Panzeri, et al. (2014). OpenQuake engine: An open hazard (and risk) software for the global earthquake model. *Seismological Research Letters*, **85**(3), 692–702.

Reasenberg, P. (1985). Second-order moment of central California seismicity, 1969–1982. *Journal of Geophysical Research: Solid Earth*, **90**(B7), 5479–5495.

Santosh, M., S. Maruyama, T. Komiya, and S. Yamamoto (2010). Orogens in the evolving Earth: from surface continents to 'lost continents' at the core–mantle boundary. *Geological Society, London, Special Publications*, **338**(1), 77–116.

Stein, R. S. (1999). The role of stress transfer in earthquake occurrence. *Nature*, **402**(6762), 605–609.

Stern, R. J. (2002). Subduction zones. *Reviews of geophysics*, **40**(4), 3–1.

Stiphout, T. van, J. Zhuang, and D. Marsan (2012). Seismicity declustering. *Community online resource for statistical seismicity analysis*, **10**(1), 1–25.

Toda, S., R. S. Stein, G. C. Beroza, and D. Marsan (2012). Aftershocks halted by static stress shadows. *Nature Geoscience*, **5**(6), 410–413.

Tsou, C.-Y., Z.-Y. Feng, and M. Chigira (2011). Catastrophic landslide induced by typhoon Morakot, Shiaolin, Taiwan. *Geomorphology*, **127**(3-4), 166–178.

Turcotte, D. L. and G. Schubert (2002). *Geodynamics*. Cambridge university press.

Uhrhammer, R. (1986). Characteristics of northern and central California seismicity. *Earthquake Notes*, **57**(1), 21.

Wesnousky, S. G. (2008). Displacement and geometrical characteristics of earthquake surface ruptures: Issues and implications for seismic-hazard analysis and the process of earthquake rupture. *Bulletin of the Seismological Society of America*, **98**(4), 1609–1632.

WHO (2023). *WHO*. [Online; accessed 03-Apr-2023]. URL: `%5Curl%7Bhttps://www.who.int/health-topics/earthquakes#tab=tab_1%7D`.

Wiemer, S. (2001). A software package to analyze seismicity: ZMAP. *Seismological Research Letters*, **72**(3), 373–382.

Wiemer, S. and M. Wyss (2000). Minimum magnitude of completeness in earthquake catalogs: Examples from Alaska, the western United States, and Japan. *Bulletin of the Seismological Society of America*, **90**(4), 859–869.

Zhuang, J., Y. Ogata, and D. Vere-Jones (2002). Stochastic declustering of space-time earthquake occurrences. *Journal of the American Statistical Association*, **97**(458), 369–380.